

# Deep Multimodal Neural Architecture Search

Zhou Yu

Hangzhou Dianzi University  
yuz@hdu.edu.cn

Meng Wang

Hefei University of Technology  
eric.mengwang@gmail.com

Yuhao Cui

Hangzhou Dianzi University  
cuiyh@hdu.edu.cn

Dacheng Tao

University of Sydney  
dacheng.tao@sydney.edu.au

Jun Yu\*

Hangzhou Dianzi University  
yujun@hdu.edu.cn

Qi Tian

Huawei  
tian.qi1@huawei.com

## ABSTRACT

Designing effective neural networks is fundamentally important in deep multimodal learning. Most existing works focus on a single task and design neural architectures manually, which are highly task-specific and hard to generalize to different tasks. In this paper, we devise a generalized deep multimodal neural architecture search (MMnas) framework for various multimodal learning tasks. Given multimodal input, we first define a set of primitive operations, and then construct a deep encoder-decoder based unified backbone, where each encoder or decoder block corresponds to an operation searched from a predefined operation pool. On top of the unified backbone, we attach task-specific heads to tackle different multimodal learning tasks. By using a gradient-based NAS algorithm, the optimal architectures for different tasks are learned efficiently. Extensive ablation studies, comprehensive analysis, and superior experimental results show that MMnasNet significantly outperforms existing state-of-the-art approaches across three multimodal learning tasks (over five datasets), including visual question answering, image-text matching, and visual grounding. Code will be made available.

## CCS CONCEPTS

• Computing methodologies → Multi-task learning; Neural networks.

## KEYWORDS

multimodal learning, neural networks, neural architecture search

## ACM Reference Format:

Zhou Yu, Yuhao Cui, Jun Yu, Meng Wang, Dacheng Tao, and Qi Tian. 2022. Deep Multimodal Neural Architecture Search. In *Proceedings of ACM Conference (Conference'17)*. ACM, New York, NY, USA, 10 pages. <https://doi.org/10.1145/nnnnnnn.nnnnnnn>

## 1 INTRODUCTION

The developments in deep neural networks enable the machine to deal with complicated multimodal learning tasks that require

\*Jun Yu is the corresponding author.

Permission to make digital or hard copies of all or part of this work for personal or classroom use is granted without fee provided that copies are not made or distributed for profit or commercial advantage and that copies bear this notice and the full citation on the first page. Copyrights for components of this work owned by others than ACM must be honored. Abstracting with credit is permitted. To copy otherwise, or republish, to post on servers or to redistribute to lists, requires prior specific permission and/or a fee. Request permissions from [permissions@acm.org](mailto:permissions@acm.org).  
*Conference'17, July 2017, Washington, DC, USA*

© 2022 Association for Computing Machinery.  
ACM ISBN 978-x-xxxx-xxxx-x/YY/MM... \$15.00  
<https://doi.org/10.1145/nnnnnnn.nnnnnnn>

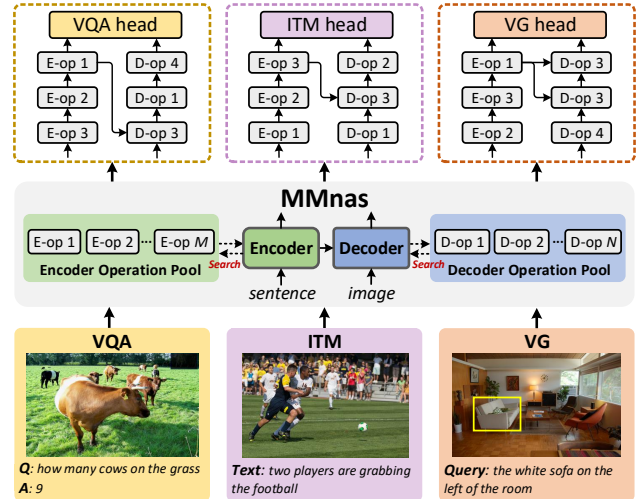


Figure 1: Schematic of the proposed generalized MMnas framework, which searches for the optimal architectures for the VQA, image-text matching, and visual grounding tasks.

a fine-grained understanding of both vision and language clues, e.g., visual captioning [1, 45], visual grounding [39, 47], image-text matching [24, 32], and visual question answering (VQA) [13, 52]. Existing approaches have pushed state-of-the-art performance on respective tasks, however, their architectures are usually dedicated to one specific task, preventing them from being generalized to other tasks. This phenomenon raises a question: *Is it possible to design a generalized framework that can simultaneously adapt to various multimodal learning tasks?*

One promising answer to this question is the *multimodal-BERT* framework [9, 28, 30, 41], which is inspired by the de facto BERT model [11] in the natural language processing (NLP) community. Using the Transformer-based architecture [43] as its backbone, BERT adopts a two-stage learning paradigm that first pre-trains a universal backbone via self-supervised learning, and then fine-tune the model for the specific task via supervised learning. Analogously, the multimodal-BERT family pre-trains the Transformer-based backbone to obtain generalizable representations from a large-scale corpus consisting of paired multimodal data (e.g., images and their associated captions). Thereafter, the generalized multimodal backbone is fine-tuned to downstream tasks such as VQA and visual grounding. Despite that the multimodal-BERT approaches deliver promising results on the benchmarks of various multimodal

learning tasks, their computational costs are usually very high (*e.g.*,  $\sim 10$ M training samples [41] or  $\sim 300$ M model size [9, 30]), which severely limits their applicability.

In this paper, we tackle the generalized multimodal learning problem from another perspective. Rather than pre-training one generalized model for various tasks, we design a generalized framework instead, which can adaptively learn the optimal architecture for various tasks. To do this, we introduce neural architecture search (NAS) [58] into multimodal learning and propose a deep multimodal neural architecture search (MMnas) framework (see Figure 1). Inspired by the modularized MCAN model [51], we first define a set of primitive operations as the basic unit to be searched. Taking image and sentence features as inputs, we design a unified encoder-decoder backbone by respectively feeding features into the encoder and decoder. The encoder (or the decoder by analogy) in the unified backbone consists of multiple encoder blocks cascaded in depth, where each block corresponds to an operation searched from the encoder operation pool. On top of the unified backbone, task-specific heads are respectively designed for each task (*e.g.*, VQA, visual grounding). By attaching the unified backbone with each head (*i.e.*, task), we use a gradient-based one-shot NAS algorithm to efficiently search the optimal composition of the operations to obtain the MMnasNet to the respective task. Compared to *hand-crafted* composition by MCAN, the *automatically searched* composition by MMnasNet can adapt better to fit the characteristics of each task and hence lead to better performance. It is worth noting that the proposed MMnasNet is not conflict with the multimodal-BERT approaches. We can also apply the pre-training strategy on MMnasNet to further enhance its performance.

To summarize, the main contributions of this study is three-fold:

- (1) We put forward a new generalized multimodal learning paradigm that uses the neural architecture search (NAS) algorithm to search for the optimal architecture for different tasks. Compared with the multimodal-BERT approaches that use large-scale data to pre-train a generalized model, our paradigm can better capture the characteristics of each task and be more parametric efficient.
- (2) We devise a novel MMnas framework, which consists of a unified encoder-decoder backbone and task-specific heads to deal with different task, including visual question answering, image-text matching, and visual grounding.
- (3) We conduct extensive experiments on five commonly used benchmark datasets. The optimal MMnasNet delivers new state-of-the-art performance, highlighting the effectiveness and generalizability of the proposed MMnas framework.

## 2 RELATED WORK

We briefly review previous studies on typical multimodal learning tasks and neural architecture search.

**Multimodal Learning Tasks:** Multimodal learning aims to build models that can understand and associate information from multiple modalities. From early research on audio-visual speech recognition [12, 55] to the recent explosion of interest in vision-and-language tasks [2, 8, 48], multimodal learning is a multi-disciplinary field of significant importance and potential. At present, multimodal learning with deep neural networks is the de facto paradigm

for modern multimodal learning tasks, such as visual question answering (VQA) [2][24][51], image-text matching [22, 27], and visual grounding [49][47]. In the following, we briefly describe three typical multimodal learning tasks and a few representative approaches accordingly.

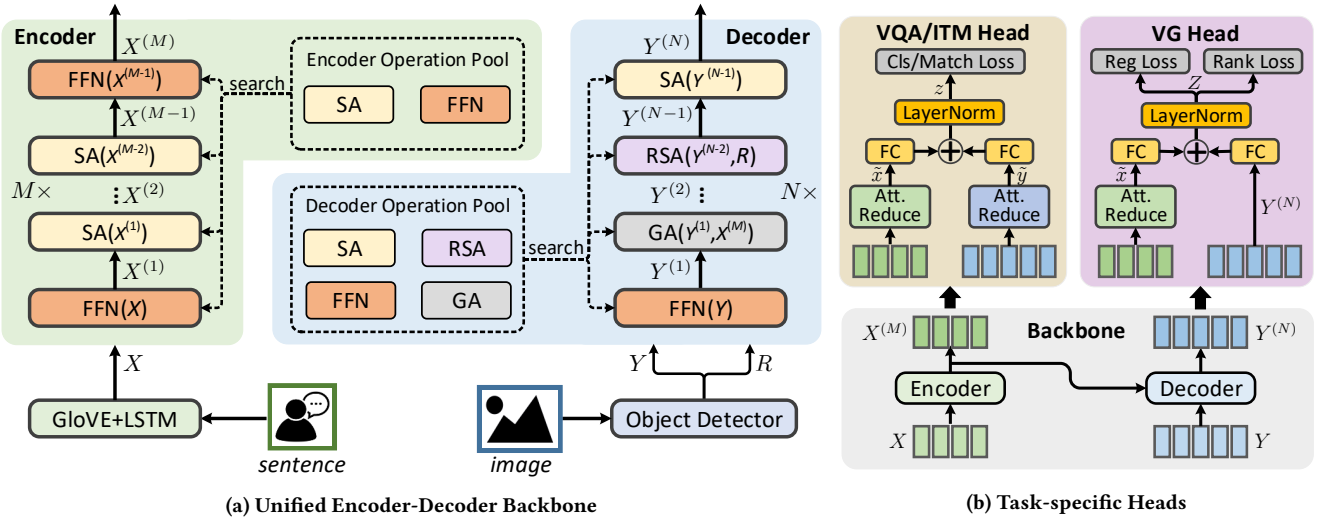
The VQA task aims to answer a question in natural language with respect to a given image, which requires a fine-grained and simultaneous understanding of both image and question. Antol *et al.* presented a large-scale VQA benchmark with human annotations and some baseline methods [2]. Fukui *et al.* [13], Kim *et al.* [25], Ben *et al.* [4], and Yu *et al.* [52] devised different approximated bilinear pooling models to effectively fuse multimodal features with second-order interactions and then integrate them with attention-based neural networks. Most recently, deep co-attention models that were proposed to integrate multimodal fusion and attention learning and delivered new state-of-the-art performance on the benchmark datasets [14, 24, 33, 51].

Image-text matching aims to learn two respective mapping functions for the image modality and the text modality, which are then projected into a common semantic space for distance measurement. Karpathy *et al.* proposed a deep fragment embedding approach to learn the fine-grained similarity between the visual object in the image and textual word in the caption by maximizing their dot-product similarity under a multi-instance learning framework [22]. Lee *et al.* proposed a stacked cross attention network to exploit the correspondences between textual words and image regions in discovering full latent alignments [27]. Wang *et al.* introduced a cross-modal message passing approach that adaptively controls the information flow across modalities to model fine-grained image-text interactions [44].

Visual grounding (*a.k.a.*, referring expression comprehension) aims to localize an object in an image referred to by a textual query. Rohrbach *et al.* proposed a GroundER model to localize the referred object by reconstructing the sentence using attention mechanism [39]. Yu *et al.* introduced a modular attention network that simultaneously models the language-based attention and visual-based attention to capture rich contextual information for accurate localization [47]. Yang *et al.* proposed a dynamic graph attention network to perform language-driven visual reasoning by modeling the relationships among the visual objects in the image and the linguistic structure of the query expression [46].

The tasks above have the same input modalities (*i.e.*, image and text), however, their solutions are diverse and task-specific, thus preventing them from being generalized to other tasks. Inspired by the success of BERT model [11] in the NLP community, multimodal-BERT approaches are proposed to learn generalized multimodal representation in a self-supervised manner [9, 28, 30, 41]. Although they have obtained promising results, they usually suffer from tremendous computational costs which limit their usability in practical scenarios.

**Neural Architecture Search:** Neural architecture search (NAS), *a.k.a.* AutoML, has drawn an increasing interest in the last couple of years, and has been successfully applied to various deep learning tasks, such as image recognition [59], object detection [15], and language modeling [40]. Early NAS methods use the reinforcement learning to search neural architectures, which are computationally exhaustive [58, 59]. Recent works accelerate the



**Figure 2: The flowchart of the MMnas framework, which consists of (a) unified encoder-decoder backbone and (b) task-specific heads on top the backbone for visual question answer (VQA), image-text matching (ITM), and visual grounding (VG). Note that the searched architecture shown in (a) is only a schematic example.**

searching process by using weight-sharing [36] or hypernetwork [6]. Although these methods bring acceleration by orders of magnitude, they require a meta-controller (e.g., a hypernetwork or an RNN) which still burdens computational speed. Recently, one-shot NAS methods have been proposed to eliminate the meta-controller by modeling the NAS problem as a single training process of an over-parameterized supernet that comprises all candidate paths [5, 7, 29].

The most closely related study to our work is the MFAS approach [35], which also incorporates NAS to search the optimal architecture for multimodal tasks. However, MFAS focuses on a simpler problem to search for the multimodal fusion model given two input features, which cannot be directly used to address the multimodal learning tasks in this paper.

### 3 THE MMNAS FRAMEWORK

In this section, we introduce a generalized multimodal learning framework MMnas via neural architecture search, which can be flexibly adapted to a wide range of multimodal learning tasks involving image-sentence inputs. As shown in Figure 2, MMnas contains a unified encoder-decoder backbone and task-specific heads. Taking an image and its associated sentence (e.g., a question, a caption or a query) as inputs, the unified encoder-decoder backbone learns the multimodal interactions with a deep modularized network consisting of stacked encoder and decoder blocks, where each block is searched within a set of predefined primitive operations. On top of the unified backbone, we design task-specific heads to deal with the VQA, image-text matching (ITM), and visual grounding (VG) tasks, respectively. Before presenting the MMnas framework, we first introduce its basic building blocks, the primitive operations.

#### 3.1 Primitive Operations

In the following, we present four types of primitive operations, termed as the *self-attention* (SA), *guided-attention* (GA), *feed-forward network* (FFN), and *relation self-attention* (RSA) operations. First, we introduce a generalized formulation of the *scaled dot-product attention* proposed in [43], which is the core of our primitive operations below.

Denote  $m$  queries and  $n$  key-value pairs as  $Q \in \mathbb{R}^{m \times d}$ ,  $K \in \mathbb{R}^{n \times d}$ ,  $V \in \mathbb{R}^{n \times d}$  respectively, where  $d$  is the common dimensionality. The original scaled dot-product attention function in [43] obtains the output features  $F \in \mathbb{R}^{m \times d}$  by weighted summation over all values  $V$  with respect to the attention learned from the scaled dot-product of  $Q$  and  $K$ :

$$F = A(Q, K, V) = \text{softmax}\left(\frac{QK^T}{\sqrt{d}}\right)V \quad (1)$$

Inspired by [20], we introduce the apriori relationship  $R \in \mathbb{R}^{m \times n}$  between  $Q$  and  $K$  into Eq.(1) to obtain a more generalized formula:

$$F = A(Q, K, V, R) = \text{softmax}\left(\frac{QK^T}{\sqrt{d}} + R\right)V \quad (2)$$

Without loss of generality, the commonly used multi-head mechanism [43] can also be incorporated with the generalized scaled dot-product attention function, which consists of  $h$  paralleled heads (i.e., independent attention functions) to further improve the representation capacity of the attended features:

$$F = \text{MHA}(Q, K, V, R) = [\text{head}_1, \text{head}_2, \dots, \text{head}_h]W^O \quad (3)$$

where each  $\text{head}_j = A(QW_j^Q, KW_j^K, VW_j^V, R)$  refers to an independent scaled dot-product attention function.  $W_j^Q, W_j^K, W_j^V \in \mathbb{R}^{d \times d_h}$  are the projection matrices for the  $j$ -th head, and  $W^O \in \mathbb{R}^{h \times d_h \times d}$ .  $d_h$  is the dimensionality of the output features from each head and is usually set to  $d_h = d/h$ .

**SA(X):** Taking a group of input features  $X \in \mathbb{R}^{m \times d_x}$  of dimension  $d_x$ , the output features  $Z \in \mathbb{R}^{m \times d}$  of the SA operation are obtained by feeding the inputs through Eq.(3) as follows:

$$Z = \text{SA}(X) = \text{MHA}(X, X, X, \mathbf{0}) \quad (4)$$

where each  $z_i \in Z$  encodes the intra-modal interactions between  $x_i$  and all features within  $X$ .  $\mathbf{0}$  is an all-zero matrix indicating that no relation prior is provided.

**GA(X, Y):** Taking two group of features  $X \in \mathbb{R}^{m \times d_x}$  and  $Y \in \mathbb{R}^{n \times d_y}$  of dimension  $d_x$  and  $d_y$  respectively, the GA operation transforms them into  $Z \in \mathbb{R}^{m \times d}$  as follows:

$$Z = \text{GA}(X, Y) = \text{MHA}(X, Y, Y, \mathbf{0}) \quad (5)$$

where each  $z_i \in Z$  encodes the inter-modal interactions between  $x_i$  and all features within  $Y$ .

**FFN(X):** This operation is a two-layer MLP network with ReLU activation and dropout in between. Taking one group of input features  $X \in \mathbb{R}^{m \times d_x}$ , the transformed output features  $Z \in \mathbb{R}^{m \times d}$  of the FFN operation are obtained as follows:

$$Z = \text{FFN}(X) = \text{FC}_d \circ \text{Drop}_{0.1} \circ \text{ReLU} \circ \text{FC}_{4d}(X) \quad (6)$$

where  $\text{FC}_d(\cdot)$  is a fully-connected layer of output dimension  $d$  and  $\text{Drop}_p(\cdot)$  is a dropout layer with dropout rate  $p$ . The symbol  $\circ$  denotes a composition of two layers.

**RSA(X, R):** This operation takes a group of features  $X \in \mathbb{R}^{m \times d_x}$  along with their relation features  $R \in \mathbb{R}^{m \times m \times d_r}$  as inputs, where  $d_r$  is the dimensionality of the relation features. The output features  $Z \in \mathbb{R}^{m \times d}$  of the RSA operation are obtained as follows:

$$\begin{aligned} \text{MLP}(R) &= \text{ReLU} \circ \text{FC}_1 \circ \text{ReLU} \circ \text{FC}_{d_h}(R) \\ Z = \text{RSA}(X, R) &= \text{MHA}(X, X, X, \log(\text{MLP}(R) + \epsilon)) \end{aligned} \quad (7)$$

where  $\text{MLP}(R)$  denotes a two-layer MLP network with transformations applied on the last axis of  $R$ .  $\epsilon = 1e^{-6}$  is a small constant to avoid the underflow problem.

Shortcut connection [19] and layer normalization [3] are applied to all primitive operations featured above. Without losing generality, more operations can be included to enlarge the operation pool seamlessly.

### 3.2 Unified Encoder-Decoder Backbone

Inspired by [51], we construct a unified encoder-decoder as the backbone to model the deep interactions between the bimodal inputs consisting of an image and its associated sentence. In the following, we describe each component of the backbone in detail.

**Sentence and Image Representations:** The input sentence is first tokenized and then trimmed (or zero-padded) into a sequence of  $m$  words. Each word is represented as a 300-D vector using the pre-trained GloVe word embeddings [34]. The word embeddings are fed into a one-layer LSTM network with  $d_x$  hidden units, resulting in the final sentence features  $X \in \mathbb{R}^{m \times d_x}$ .

Following the strategy in [1], the input image is represented as a set of objects extracted from a pre-trained object detection model (e.g., Faster R-CNN). For each image, the object detector predicts  $n$  objects with each object being represented as a group of visual features and relation features, respectively. The visual features  $Y \in \mathbb{R}^{n \times d_y}$  are obtained by pooling the convolutional features

from the detected objects. The relation features  $R \in \mathbb{R}^{n \times n \times 4}$  are calculated by the relative spatial relationships of object pairs<sup>1</sup>.

**Sentence Encoder and Image Decoder:** Taking the word-level sentence features  $X$  as inputs, the sentence encoder learns the intra-modal interactions of sentence words by passing  $X$  through  $M$  encoder blocks  $\{b_{\text{enc}}^{(1)}, b_{\text{enc}}^{(2)}, \dots, b_{\text{enc}}^{(M)}\}$  recursively:

$$X^{(i)} = b_{\text{enc}}^{(i)}(X^{(i-1)}) \quad (8)$$

where  $i \in \{1, 2, \dots, M\}$  and  $X^{(0)} = X$ . Each  $b_{\text{enc}}^{(i)}(\cdot)$  corresponds to an operation searched from an encoder operation pool with independent operation weights. Similar to [51], the encoder operation pool consists of two candidate operations: SA and FFN.

Analogous to the sentence encoder, we design an image decoder consisting of  $N$  decoder blocks  $\{b_{\text{dec}}^{(1)}, b_{\text{dec}}^{(2)}, \dots, b_{\text{dec}}^{(N)}\}$ . Slightly different from that of the encoder, the decoder operation pool contains four operations: SA, RSA, GA, and FFN. Taking the visual features  $Y$  and relation features  $R$  from the image, along with the output features  $X^{(M)}$  from the sentence encoder as inputs, the image decoder models the intra- and inter-modal interactions of the multimodal inputs in a recursive manner:

$$Y^{(i)} = b_{\text{dec}}^{(i)}(Y^{(i-1)}, R, X^{(M)}) \quad (9)$$

where  $i \in \{1, 2, \dots, N\}$  and  $Y^{(0)} = Y$ . Each  $b_{\text{dec}}^{(i)}(\cdot)$  takes at least one input (i.e.,  $Y^{(i-1)}$ ) and may have an additional input (i.e.,  $R$  or  $X^{(M)}$ ) if specific operation is searched (i.e., RSA or GA).

### 3.3 Task-specific Heads

The output sentence features  $X^{(M)} = [x_1^{(M)}, x_2^{(M)}, \dots, x_m^{(M)}]$  and image features  $Y^{(N)} = [y_1^{(N)}, y_2^{(N)}, \dots, y_n^{(N)}]$  from the unified encoder-decoder backbone contain rich information about the attentive interactions between the sentence words and image objects. On top of the backbone, we attach task-specific heads to address the visual question answering (VQA), image-text matching (ITM), and visual grounding (VG) tasks, respectively.

**VQA Head:** Similar to most existing works [2, 24, 52], we resolve the VQA problem by predicting the best-matched answer to the question from a large answer vocabulary. Inspired by the multi-modal fusion model in [51], we use two independent attentional reduction models for  $X^{(M)}$  and  $Y^{(N)}$  to obtain their reduced features  $\tilde{x}$  and  $\tilde{y}$ , respectively:

$$\begin{aligned} \alpha &= \text{softmax}(\text{MLP}(X^{(M)})), & \beta &= \text{softmax}(\text{MLP}(Y^{(N)})) \\ \tilde{x} &= \sum_{i=1}^m \alpha_i x_i^{(M)}, & \tilde{y} &= \sum_{i=1}^n \beta_i y_i^{(N)} \end{aligned} \quad (10)$$

where  $\alpha \in \mathbb{R}^m, \beta \in \mathbb{R}^n$  are the attention weights to be learnt.  $\text{MLP}(X) = \text{FC}_1 \circ \text{ReLU} \circ \text{FC}_d(X)$  corresponds to a two-layer MLP network. After that, the reduced features are fused together as follows:

$$z = \text{LayerNorm}(W_x^T \tilde{x} + W_y^T \tilde{y}) \quad (11)$$

<sup>1</sup>Denote the location of the  $i$ -th object as  $\{x_i, y_i, h_i, w_i\}$ , where  $x_i, y_i$  refer to the center of the object, and  $w_i, h_i$  refer to the width and height of the object, respectively. Following the strategy in [20], the 4-D relation feature between the  $m$ -th object and the  $n$ -th object is defined as  $[\log(|x_m - x_n|/w_m), \log(|y_m - y_n|/h_m), \log(w_n/w_m), \log(h_n/h_m)]$ .

where  $W_x, W_y \in \mathbb{R}^{d \times d_z}$  are two projection matrices to embed the input features into a  $d_z$ -dimensional common space. LayerNorm is appended on the fused feature to stabilize training [3].

The fused feature  $z$  is then projected into a vector  $p \in \mathbb{R}^k$  and then fed into a  $k$ -way classification loss, where  $k$  denotes the size of the answer vocabulary. For the dataset that provides multiple answers to each question, we formulate it as a multi-label classification problem and use binary cross-entropy (BCE) loss to train the model. For the dataset that only has one answer to each question, we regard it as a single-label classification problem and use the softmax cross-entropy loss instead.

**ITM Head:** Image-text matching aims to learn a matching score to measure the cross-modal similarity between the image-text pair. Since the outputs of the ITM and VQA tasks are similar, we therefore reuse part of the model in the VQA head. On top of the fused feature  $z$  from Eq.(11), the matching score  $s \in (0, 1)$  is obtained as follows:

$$s = \sigma(W_z^T z) \quad (12)$$

where  $W_z \in \mathbb{R}^{d_z}$  and  $\sigma(\cdot)$  denotes the sigmoid function. Denote the predicted matching score of an input image-text pair as  $s(I, \mathcal{T})$ , where  $(I, \mathcal{T})$  represents a positive sample with correspondence. We use BCE loss with hard negatives mining for  $(I, \mathcal{T})$  as our loss function to train the matching model:

$$\begin{aligned} \mathcal{L}_{\text{match}} = & \log(s(I, \mathcal{T})) + \log(1 - s(I, \mathcal{T}')) \\ & + \log(s(I, \mathcal{T})) + \log(1 - s(I', \mathcal{T})) \end{aligned} \quad (13)$$

where  $\mathcal{T}'$  and  $I'$  denote the hard negative text and image samples for  $(I, \mathcal{T})$  mined from the whole training set per training epoch.

**VG Head:** We address the visual grounding task by predicting a ranking score and a refined bounding box for each visual object in the image referred to by the query. To do this, we first feed the word-level query features  $X^{(M)}$  into the attentional reduction model in Eq.(10) to obtain the reduced feature vector  $\tilde{x}$ . After that,  $\tilde{x}$  is broadcasted and integrated with the object-level image features  $Y^{(N)}$  as follows:

$$Z = \text{LayerNorm}(W_x^T \tilde{x} + W_y^T Y^{(N)}) \quad (14)$$

where  $Z \in \mathbb{R}^{n \times d_z}$  correspond to the fused features of  $n$  objects in the image. Each object feature  $z \in Z$  is then linearly projected into a ranking score  $s \in \mathbb{R}$  and a 4-D bounding box offset  $b \in \mathbb{R}^4$ , respectively. Similar to [54], we design a multi-task loss function consisting of a ranking loss  $\mathcal{L}_{\text{rank}}$  and a regression loss  $\mathcal{L}_{\text{reg}}$ :

$$\mathcal{L} = \mathcal{L}_{\text{rank}} + \lambda \mathcal{L}_{\text{reg}} \quad (15)$$

where  $\lambda$  is a hyper-parameter to balance the two terms. The  $\mathcal{L}_{\text{rank}}$  term penalizes the KL-divergence between the predicted scores  $S = [s_1, s_2, \dots, s_n] \in \mathbb{R}^n$  and the ground-truth scores  $S^* \in \mathbb{R}^n$  for  $n$  objects, where  $S^*$  are obtained by calculating the IoU scores of all objects with respect to the unique ground-truth bounding box. Softmax normalizations are respectively applied to  $S$  and  $S^*$  to form a score distribution. The  $\mathcal{L}_{\text{reg}}$  term penalizes the smoothed  $L_1$  distance [16] between the predicted offset  $b$  and the ground-truth offset  $b^*$  for the objects with their IoU scores  $S^*$  larger than a threshold  $\sigma$ . The offset  $b^* \in \mathbb{R}^4$  is obtained by calculating the translations between the bounding box of the input object and the bounding box of ground-truth object [16].

## 4 SEARCH ALGORITHM

To obtain the optimal MMnasNet architecture for each task on specific dataset, we introduce an efficient one-shot search algorithm that search the optimal architecture within an over-parameterized supernet with weight sharing.

Denote a supernet as  $\mathcal{N}(\mathcal{A}(\theta), W)$  that encodes the whole search space  $\mathcal{A}$  of MMnas, where  $W$  and  $\theta$  correspond to the model weights and architecture weights of all the possible operations in the supernet, respectively<sup>2</sup>. The optimal architecture is obtained by minimizing the expectation with respect to  $\theta$  and  $W$  jointly:

$$(\theta^*, W^*) = \underset{\theta, W}{\text{argmin}} \mathbb{E}_{a \sim \mathcal{A}(\theta)} [\mathcal{L}(\mathcal{N}(a, W))] \quad (16)$$

where  $\mathcal{L}(\cdot)$  represents the loss function applied on the training set for each task.  $a$  refers to a valid architecture sampled from the search space.  $W_a$  refers to the model weights of the architecture  $a$  inherited from  $W$  in a *weight sharing* strategy. Based on  $\theta^*$ , the optimal architecture  $a^*$  is obtained by selecting the operation with the largest architecture weight in each block of the backbone.

Inspired by the strategy in [7], we adopt an iterative algorithm to optimize the architecture weights  $\theta$  and the model weights  $W$  alternatively. We first separate the training set into two non-overlapping sets  $\mathcal{D}_m$  and  $\mathcal{D}_a$ . When training the model weights  $W$ , we first freeze the architecture weights  $\theta$  and stochastically sample exactly one operation for each block with respect to  $\theta$  after softmax activation, which results in a valid architecture  $a$ . After that, we update the model weights  $W$  activated by  $a$  via standard gradient descent on  $\mathcal{D}_m$ . When training the architecture weights  $\theta$ , we freeze the model weights  $W$ , sample a valid architecture  $a$ , and then update  $\theta$  via gradient descent on  $\mathcal{D}_a$ .

As claimed in [10], the iterative optimization of  $W$  and  $\theta$  inevitably introduces bias to certain architectures and leave the rest ones poorly optimized. To alleviate the problem, we introduce an additional *warming-up* stage before the iterative optimization. In the warming-up stage, we do not train the architecture weights  $\theta$  and sample operations uniformly to train the model weights  $W$ . This ensures that the model weights  $W$  are well initialized thus leading to more impartial and robust architecture search.

The detailed search algorithm is illustrated in Algorithm 1.

## 5 EXPERIMENTS

We evaluate the searched MMnasNets on three multimodal learning tasks and perform thorough comparative analysis to the state-of-the-art methods on five benchmark datasets. Furthermore, we conduct comprehensive ablation experiments to explore the reasons why MMnas is effective. The statistics and evaluation metrics of the datasets are shown in Table 1.

### 5.1 Experimental Setup

**Universal Setup:** We use the following hyper-parameters for MMnasNet as the default settings unless otherwise stated. For each primitive operation, the latent dimensionality in the multi-head attention  $d$  is 512 and the number of heads  $h$  is 8. The dimensionality

<sup>2</sup>Given a MMnas supernet consisting of  $M$  encoder blocks and  $N$  decoder blocks, the size of the search space is  $2^M \times 4^N$  and the number of all the possible operations in the supernet is  $2M+4N$ , where 2 and 4 correspond to the sizes of the encoder and decoder operation pools, respectively.

**Algorithm 1:** Search Algorithm for MMnasNet.

**Input:** A supernet parameterized by the architecture weights  $\theta$  and the model weights  $W$ . Training set  $\mathcal{D}_a$  and  $\mathcal{D}_m$  are used to optimize  $\theta$  and  $W$ , respectively.  $T_w$  and  $T_j$  denote the number of epochs for the warming-up and iterative optimization stages, respectively.  $u$  is a factor to balance the update frequencies of  $\theta$  and  $W$ .

**Output:** The searched optimal architecture  $a^*$

Random initialize  $\theta$  and  $W$ ;

# The warming-up stage;

**for**  $t = 1$  to  $T_w$  **do**

    Random sample an architecture  $a \sim \mathcal{A}$ ;

    Random sample a mini-batch  $d_m \subseteq \mathcal{D}_m$ ;

    Update  $W$  by descending  $\nabla_W \mathcal{L}_{\text{train}}(\mathcal{N}(a, W)$  on  $d_m$ ;

**end**

# The iterative optimization stage;

**for**  $t = 1$  to  $T_j$  **do**

**for**  $i = 1$  to  $u$  **do**

        Random sample a mini-batch  $d_m \subseteq \mathcal{D}_m$ ;

        Sample an architecture  $a \sim \mathcal{A}(\theta)$  with respect to  $\theta$ ;

        Update  $W$  by descending  $\nabla_W \mathcal{L}_{\text{train}}(\mathcal{N}(a, W)$  on  $d_m$ ;

**end**

    Random sample a mini-batch  $d_a \subseteq \mathcal{D}_a$ ;

    Sample an architecture  $a \sim \mathcal{A}(\theta)$  with respect to  $\theta$ ;

    Update  $\theta$  by descending  $\nabla_\theta \mathcal{L}_{\text{train}}(\mathcal{N}(a, W)$  on  $d_a$ ;

**end**

Return  $a^*$  by picking the operation with the largest value in  $\theta^*$  for each block.

of the fused features  $d_z$  is set to  $2d$ . The number of encoder blocks  $M$  and decoder blocks  $N$  are respectively set to 12 and 18 to match the number of blocks in the 6-layer MCAN model<sup>3</sup> [51].

For each dataset, we use its train split to perform architecture search. The train set is further random split into two subsets  $D_m$  and  $D_a$  with  $|D_m|/|D_a| = 4$ . Each randomly initialized model is warmed-up for  $T_w = 50$  epochs and then searched for another  $T_j = 20$  epochs with a mini-batch size 256. For both the warming-up and searching stages, the early stopping strategy is used if the accuracy on the validation set does not improve for 5 epochs. Adam solver with  $\beta_1 = 0$  and  $\beta_2 = 0.999$  is used as the optimizer [26]. The frequency ratio  $u$  for updating the model and architecture weights is set to 5. With the searched optimal architecture, we train the MMnasNet model again from scratch to obtain the final model. All the experiments below are conducted on a workstation with 4 Titan-V GPUs. The searching process for the models takes 10~120 GPU hours for different tasks with multi-GPU parallelization.

**VQA Setup:** For VQA-v2, we follow the setting in [51] that all questions are processed to a maximum length of  $m = 14$  and the size of the answer vocabulary is set to 3129. The visual features and relation features are extracted from a pre-trained Faster R-CNN model on Visual Genome [1]. The number of extracted objects  $n \in [10, 100]$  is determined by a confidence threshold.

**ITM Setup:** For Flickr30K, we follow the strategy in [22] to split the data into 29K/1K/1K training/validation/test images. The maximum length of texts (*i.e.*, captions) is set to  $m = 50$ . The visual features and relation features are extracted from a Faster R-CNN model pre-trained on Visual Genome with the number of objects  $n = 36$  [1]. For each positive image-text pair  $(\mathcal{I}, \mathcal{T})$  in the training set, we use the following hard sample mining strategy before each training epoch: we randomly sample 64 negative images per text and 64

<sup>3</sup>A  $L$ -layer MCAN model corresponds to a special case of the MMnasNet model consisting of  $2L$  encoder blocks (with repeated SA-FFN operations) and  $3L$  decoder blocks (with repeated SA-GA-FFN operations).

**Table 1: The detailed statistics and evaluation metrics of the tasks and datasets.**

Task	Dataset	Image Source	#Img.	#Sent.	Metric
VQA	VQA-v2 [17]	COCO	204K	1.1M	Accuracy
VG	RefCOCO [23]	COCO	20K	142K	Accuracy
	RefCOCO+ [23]		20K	142K	
	RefCOCOg [31]		26K	95K	
ITM	Flickr30K [37]	Flickr	31K	155K	Recall@K

negative texts per image from the whole training set to generate negative image-text pairs. Thereafter, we feed all these negative pairs to the current model checkpoint to predict their matching scores and regard the top-5 ranked negative samples as the hard negative samples according to their scores. Finally, we randomly pick one hard image sample  $\mathcal{I}'$  and one hard text sample  $\mathcal{T}'$  from the candidate hard negative samples, respectively.

**VG Setup:** We use the same settings for the three visual grounding datasets. For the textual queries, the maximum length is set to  $m = 14$ . For the images, we adopt two pre-trained object detectors to extract the visual features: 1) a Mask R-CNN model trained on COCO [18]; and 2) a Faster R-CNN model trained on Visual Genome [38]. During the training data preparation for the two detectors, we excluded all the images that exist in the training, validation and testing sets of RefCOCO, RefCOCO+, and RefCOCOg to avoid the data leakage problem. For both detectors above, we detect  $n = 100$  objects for each image to extract the visual and relation features. The loss weight  $\lambda$  is set to 1.

## 5.2 Ablation Experiments

We run a number of ablations experiments on VQA-v2 to analyze the reason behind MMnasNet’s effectiveness. Results shown in Table 2 and Figure 3 are discussed in detail next.

**Search Space:** In Table 2a, we compare the MMnasNet models searched from different decoder operation pools. From the results, we can see that: 1) modeling the intra-modal attention among visual objects by SA or RSA is vital to object counting performance (*i.e.*, the *number* type answers), which is consistent with the results reported in [51]; 2) introducing the RSA operation which models the relative spatial relationships between paired objects can further facilitate the object counting performance; and 3) SA and RSA are complementary to each other, hence modeling them together leads to the best performance on all answer types.

**Model Depth:** In Table 2b, we compare MMnasNet to the reference MCAN model [51] under different model depths (*i.e.*, number of encoder blocks  $M$  and decoder blocks  $N$ ). The results reveal that: 1) MMnasNet consistently outperforms MCAN, especially when the model depth is relatively shallow (*e.g.*,  $M \leq 8$ ). This can be explained that the optimal architectures for different model depths are quite different; 2) with the same  $M$  and  $N$ , the model size of MMnasNet is slightly larger than MCAN. This is because MMnasNet tends to use more FFN operations, which introduces more parameters to increase the nonlinearity of the model; and 3) with the increase of model depth, both MCAN and MMnasNet saturate at  $M=12$  and  $N=18$ , which reflects the bottleneck of the used deep encoder-decoder framework.



Decoder operations	All	Y/N	Num	Other
{GA, FFN}	66.5	84.9	45.2	58.2
{SA, GA, FFN}	67.4	85.0	49.7	58.7
{RSA, GA, FFN}	67.6	84.9	51.3	58.8
{SA, RSA, GA, FFN}	<b>67.8</b>	<b>85.1</b>	<b>52.1</b>	<b>58.9</b>

(a) *Search Space*: Per-type accuracies of MMnasNet with different decoder operation pools. All models use the same encoder operation pool of {SA, FFN}.

$M$	$N$	MCAN (Size)	MMnasNet (Size)
4	6	66.1 (27M)	67.1 (28M)
8	12	66.9 (41M)	67.7 (44M)
12	18	67.2 (56M)	<b>67.8</b> (58M)
16	24	67.2 (68M)	67.7 (76M)

(b) *Model Depth*: Overall accuracies and sizes of MCAN and MMnasNet with different number of encoder blocks  $M$  and decoder blocks  $N$ .

Encoder	Decoder	Accuracy
R	R	66.9
S	R	67.1
R	S	67.6
S	S	<b>67.8</b>

(c) *Random vs. Searched*: Overall accuracies of MMnasNet with random (R) or searched (S) architecture for the encoder-decoder.

**Table 2: Ablation experiments for MMnasNet on VQA-v2. We train on the *train* split and report the results on the *val* split.**

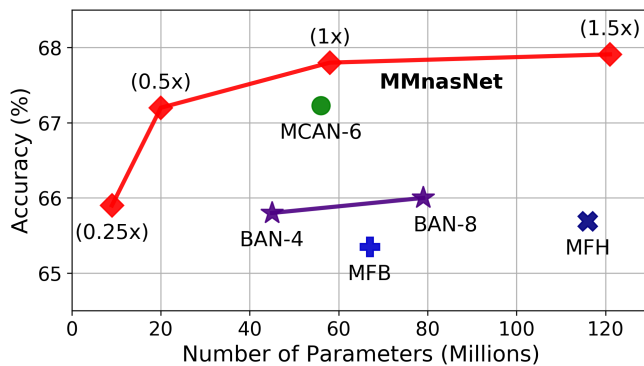


**Figure 3: Model Size vs. Accuracy.** All results are reported on the *val* split of VQA-v2. For MMnasNet, we use the scaling factors {0.25x, 0.5x, 1x, 1.5x} with respect to  $d = 512$ .

**Random vs. Searched:** To prove the necessity and superiority of the searched architectures over randomly generated ones, we conduct the experiments in Table 2c by alternatively using the searched or random architectures for the encoder and decoder, respectively. From the results, we can see that: 1) the searched architectures outperforms the random counterparts by up to 0.9 points; 2) the design of the decoder architecture is much more important than the encoder architecture; and 3) the all-random architecture also performs well compared to some recent works [14, 24]. This suggests the used primitive operations that constitute the architecture also play a key role in model performance.

**Efficiency vs. Accuracy:** With the optimal MMnasNet architecture ( $M=12$  and  $N=18$ ), we explore the trade-off between efficiency and accuracy by training MMnasNet variants with different latent dimensionality  $d$ . By setting the variant with  $d=512$  as the reference model (1x), we vary the scaling factors {0.25x, 0.5x, 1.5x} with respect to  $d$  and report the parameters-accuracy results in Figure 3. We can see that: 1) the reference MMnasNet (1x) model steadily outperforms all the existing state-of-the-art methods by 0.6~2.6 points with about 60M parameters, showing the parametric efficiency of MMnasNet; 2) with only 1/3 number of parameters, MMnasNet (0.5x) is still competitive with MCAN-6; 3) MMnasNet (1.5x) brings only 0.1 point improvement over the reference model at the expense of twice the model size; and 4) MMnasNet (0.25x) obtains a very compact model at the expense of a dramatical accuracy drop. Therefore, we use MMnasNet (1x) and MMnasNet

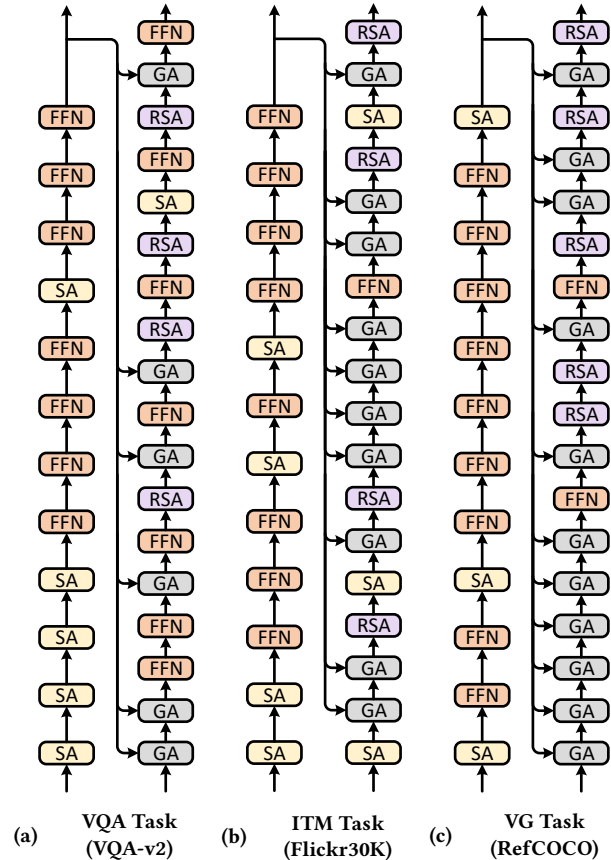


**Figure 4: The optimal MMnasNet backbones searched for different tasks (over specific datasets).**

(0.5x) in the following experiments to compare with the state-of-the-art models.

### 5.3 Main Results

Taking the ablation studies into account, we compare the best-performing MMnasNet models (with  $M=12$  and  $N=18$ ) to the state-of-the-art approaches on five benchmark datasets. In addition to the standard MMnasNet (1x) model, we also report the results of the compact MMnasNet (0.5x) model on each dataset. Figure 4 illustrates the optimal MMnasNet backbones searched for different

**Table 4: Accuracies (with IoU>0.5) on RefCOCO, RefCOCO+ and RefCOCOg to compare with the state-of-the-art methods. All methods use detected objects to extract visual features.**

Method	Size	Object Detector			RefCOCO			RefCOCO+			RefCOCOg	
		Dataset	Model	Backbone	TestA	TestB	Val	TestA	TestB	Val	Test	Val
VC [56]	-	COCO	FRCN	VGG-16	73.3	67.4	-	58.4	53.2	-	-	-
Spe.+Lis.+Rein.+MMI [49]	-	COCO	SSD	VGG-16	73.7	65.0	69.5	60.7	48.8	55.7	59.6	60.2
Spe.+Lis.+Rein.+MMI [49]	-	COCO	SSD	VGG-16	73.1	64.9	69.0	60.0	49.6	54.9	59.2	59.3
MAttNet [47]	14M	COCO	MRCN	ResNet-101	81.1	70.0	76.7	71.6	56.0	65.3	67.3	66.6
DDPN [54]	10M	Genome	FRCN	ResNet-101	80.1	72.4	76.8	70.5	54.1	64.8	67.0	66.7
MUAN-10 [50]	75M	Genome	FRCN	ResNet-101	86.5	78.7	82.8	79.5	64.3	73.2	74.3	74.2
MMnasNet (0.5×)	16M	COCO	MRCN	ResNet-101	82.7	<b>79.2</b>	80.9	70.4	62.5	68.8	71.2	71.7
MMnasNet (1×)	52M	COCO	MRCN	ResNet-101	82.5	78.4	81.5	70.9	62.3	69.8	72.7	73.1
MMnasNet (1×)	52M	Genome	FRCN	ResNet-101	<b>87.4</b>	77.7	<b>84.2</b>	<b>81.0</b>	<b>65.2</b>	<b>74.7</b>	<b>75.7</b>	<b>74.7</b>

**Table 3: Accuracies on the test-dev and test-std splits of VQA-v2 to compare with the state of the arts approaches. All methods use the same visual features [1] and are trained on the train+val+vg splits, where vg denotes the augmented dataset from Visual Genome.**

Method	Size	Dev				Std
		All	Y/N	Num	Other	All
Bottom-Up [42]	22M	65.32	81.82	44.21	56.05	65.67
MFH+CoAtt [53]	116M	68.76	84.27	49.56	59.89	-
BAN-8 [24]	79M	69.52	85.31	50.93	60.26	-
BAN-8 (+G+C) [24]	90M	70.04	85.42	54.04	60.52	70.35
DFAF-8 [14]	114M	70.22	86.09	53.32	60.49	70.34
MCAN-6 [51]	58M	70.63	86.82	53.26	60.72	70.90
MUAN-10 [50]	83M	70.82	86.77	54.40	60.89	71.10
MMnasNet (0.5×)	20M	70.44	86.35	55.53	60.21	-
MMnasNet (1×)	58M	<b>71.24</b>	<b>87.27</b>	<b>55.68</b>	<b>61.05</b>	<b>71.46</b>

tasks (over specific datasets). This verifies our hypothesis that the optimal architectures for different tasks may vary prominently. Note that we do not compare MMnasNet to the multimodal-BERT approaches (e.g., LXMRET [41] or UNITER [9]), since they introduce additional training datasets for model pre-training thus may lead to unfair comparison.

In Table 3, we compare MMnasNets to the state-of-the-art methods on VQA-v2. The demonstrated results show that: 1) with 1/4~1/3 model size, MMnasNet (0.5×) model achieves competitive performance to the previous state-of-the-art models; and 2) with nearly the same model size, MMnasNet (1×) outperforms existing top performance approaches by a clear margin on all answer types.

In Table 4, we report the comparative results on RefCOCO, RefCOCO+, and RefCOCOg, respectively. We use the commonly used accuracy metric [47], where a prediction is considered to be correct if the predicted bounding box overlaps with the ground-truth of IoU > 0.5. With the standard visual features (i.e., MRCN pre-trained on COCO), MMnasNet (0.5×) significantly outperforms the previous state-of-the-art MAttNet model [47] with a similar model size, and MMnasNet (1×) obtain slight improvement over MMnasNet (0.5×) on RefCOCO+ and RefCOCOg. Be equipped

**Table 5: Recall@{1, 5, 10} on Flickr30K to compare with the state-of-the-art methods.**

Method	Text→Image			Image→Text		
	R@1	R@5	R@10	R@1	R@5	R@10
DAN [32]	55.0	81.8	89.0	39.4	69.2	79.1
DPC [57]	55.6	81.9	89.5	39.1	69.2	80.9
SCO [21]	55.5	82.0	89.3	41.1	70.5	80.1
SCAN <sub>t→i</sub> [27]	61.8	87.5	93.7	45.8	74.4	83.0
SCAN <sub>i→t</sub> [27]	67.7	88.9	94.0	44.0	74.2	82.6
CAMP [44]	68.1	89.7	95.2	51.5	77.1	85.3
MMnasNet (0.5×)	77.1	92.8	96.1	59.6	84.9	90.1
MMnasNet (1×)	<b>78.3</b>	<b>94.6</b>	<b>97.4</b>	<b>60.7</b>	<b>85.1</b>	<b>90.5</b>

with the powerful visual features (i.e., FRCN pre-trained on Visual Genome), MMnasNet (1×) obtains remarkable improvement and delivers the new state-of-the-art performance across all datasets.

Table 5 contains the image-text matching results on Flickr30K. Similar to most existing works [27, 44], we report the matching results in terms of Recall@K, where K denotes the top-K results retrieved from a database and ranges within {1, 5, 10}. The cross-modal matching results from two directions, i.e., image-to-texts and text-to-images, are demonstrated in Table 5 to compare with the state-of-the-art approaches. From the results, we can see that MMnasNet (0.5×) significantly outperforms existing state-of-the-art methods in terms of all evaluation metrics. Furthermore, the standard MMnasNet (1×) model steadily outperforms the compact (0.5×) model as expected. Since the model sizes of MMnasNets do not change much across different tasks, we do not report them further due to space limitations.

## 6 CONCLUSION

In this paper, we present a generalized deep multimodal neural architecture search (MMnas) framework for various multimodal learning tasks. Different from the existing approaches that design hand-crafted and task-specific architectures to address only a single task, MMnas can be generalized to automatically learn the optimal architectures of different tasks. To achieve this, we construct a unified encoder-decoder backbone with each encoder/decoder



block corresponding to an operation searched from a candidate set of predefined operations. On top of the unified backbone, we attach task-specific heads to deal with different tasks. The optimal architecture for each task is learned by an efficient neural architecture search (NAS) algorithm to obtain task-specific MMnasNet. Extensive experiments are conducted on the VQA, visual grounding, and image-text matching tasks to show the generalizability and effectiveness of the proposed MMnas framework. Comprehensive results from five benchmark datasets validate the superiority of MMnasNet over existing state-of-the-art methods.

Different from existing multimodal-BERT approaches that use large-scale multimodal pre-training, we introduce an alternative way to address the generalized multimodal learning problem via a NAS framework. We hope our work may serve as a solid baseline to inspire future research on multimodal learning.

## REFERENCES

- [1] Peter Anderson, Xiaodong He, Chris Buehler, Damien Teney, Mark Johnson, Stephen Gould, and Lei Zhang. 2018. Bottom-Up and Top-Down Attention for Image Captioning and Visual Question Answering. *IEEE Conference on Computer Vision and Pattern Recognition (CVPR)* (2018).
- [2] Stanislaw Antol, Aishwarya Agrawal, Jiasen Lu, Margaret Mitchell, Dhruv Batra, C Lawrence Zitnick, and Devi Parikh. 2015. Vqa: Visual question answering. In *IEEE International Conference on Computer Vision (ICCV)*. 2425–2433.
- [3] Jimmy Lei Ba, Jamie Ryan Kiros, and Geoffrey E Hinton. 2016. Layer normalization. *arXiv preprint arXiv:1607.06450* (2016).
- [4] Hedi Ben-Younes, Rémi Cadene, Matthieu Cord, and Nicolas Thome. 2017. Mutan: Multimodal tucker fusion for visual question answering. In *IEEE International Conference on Computer Vision (ICCV)*.
- [5] Gabriel Bender, Pieter-Jan Kindermans, Barret Zoph, Vijay Vasudevan, and Quoc Le. 2018. Understanding and Simplifying One-Shot Architecture Search. In *International Conference on Machine Learning (ICML)*. 550–559.
- [6] Andrew Brock, Theodore Lim, James Millar Ritchie, and Nicholas J Weston. 2018. SMASH: One-Shot Model Architecture Search through HyperNetworks. In *International Conference on Learning Representations (ICLR)*.
- [7] Han Cai, Ligeng Zhu, and Song Han. 2018. Proxylessnas: Direct neural architecture search on target task and hardware. *arXiv preprint arXiv:1812.00332* (2018).
- [8] Xinlei Chen, Hao Fang, Tsung-Yi Lin, Ramakrishna Vedantam, Saurabh Gupta, Piotr Dollár, and C Lawrence Zitnick. 2015. Microsoft coco captions: Data collection and evaluation server. *arXiv preprint arXiv:1504.00325* (2015).
- [9] Yen-Chun Chen, Linjie Li, Licheng Yu, Ahmed El Kholy, Faisal Ahmed, Zhe Gan, Yu Cheng, and Jingjing Liu. 2019. Uniter: Learning universal image-text representations. *arXiv preprint arXiv:1909.11740* (2019).
- [10] Xiangxiang Chu, Bo Zhang, Ruijun Xu, and Jixiang Li. 2019. Fairnas: Rethinking evaluation fairness of weight sharing neural architecture search. *arXiv preprint arXiv:1907.01845* (2019).
- [11] Jacob Devlin, Ming-Wei Chang, Kenton Lee, and Kristina Toutanova. 2019. BERT: Pre-training of Deep Bidirectional Transformers for Language Understanding. In *Conference of the NAACL-HLT*. 4171–4186.
- [12] Stéphane Dupont and Juergen Luetttin. 2000. Audio-visual speech modeling for continuous speech recognition. *IEEE Transactions on Multimedia* 2, 3 (2000), 141–151.
- [13] Akira Fukui, Dong Huk Park, Daylen Yang, Anna Rohrbach, Trevor Darrell, and Marcus Rohrbach. 2016. Multimodal Compact Bilinear Pooling for Visual Question Answering and Visual Grounding. *Conference on Empirical Methods in Natural Language Processing (EMNLP)* (2016).
- [14] Peng Gao, Zhengkai Jiang, Haoxuan You, Pan Lu, Steven CH Hoi, Xiaogang Wang, and Hongsheng Li. 2019. Dynamic fusion with intra-and inter-modality attention flow for visual question answering. In *IEEE Conference on Computer Vision and Pattern Recognition (CVPR)*. 6639–6648.
- [15] Golnaz Ghiasi, Tsung-Yi Lin, and Quoc V Le. 2019. Nas-fpn: Learning scalable feature pyramid architecture for object detection. In *IEEE Conference on Computer Vision and Pattern Recognition (CVPR)*. 7036–7045.
- [16] Ross Girshick. 2015. Fast r-cnn. In *IEEE International Conference on Computer Vision (ICCV)*. 1440–1448.
- [17] Yash Goyal, Tejas Khot, Douglas Summers-Stay, Dhruv Batra, and Devi Parikh. 2017. Making the V in VQA Matter: Elevating the Role of Image Understanding in Visual Question Answering. *IEEE Conference on Computer Vision and Pattern Recognition (CVPR)* (2017).
- [18] Kaiming He, Georgia Gkioxari, Piotr Dollár, and Ross Girshick. 2017. Mask r-cnn. In *IEEE Conference on Computer Vision and Pattern Recognition (CVPR)*. 2961–2969.
- [19] Kaiming He, Xiangyu Zhang, Shaoqing Ren, and Jian Sun. 2016. Deep residual learning for image recognition. *IEEE Conference on Computer Vision and Pattern Recognition (CVPR)* (2016).
- [20] Han Hu, Jiayuan Gu, Zheng Zhang, Jifeng Dai, and Yichen Wei. 2018. Relation networks for object detection. In *IEEE Conference on Computer Vision and Pattern Recognition (CVPR)*. 3588–3597.
- [21] Yan Huang, Qi Wu, Chunfeng Song, and Liang Wang. 2018. Learning semantic concepts and order for image and sentence matching. In *IEEE Conference on Computer Vision and Pattern Recognition (CVPR)*. 6163–6171.
- [22] Andrej Karpathy and Li Fei-Fei. 2015. Deep visual-semantic alignments for generating image descriptions. In *IEEE Conference on Computer Vision and Pattern Recognition (CVPR)*. 3128–3137.
- [23] Sahar Kazemzadeh, Vicente Ordonez, Mark Matten, and Tamara Berg. 2014. Referitgame: Referring to objects in photographs of natural scenes. In *Conference on Empirical Methods in Natural Language Processing (EMNLP)*. 787–798.
- [24] Jin-Hwa Kim, Jaehyun Jun, and Byoung-Tak Zhang. 2018. Bilinear attention networks. In *Advances in Neural Information Processing Systems (NIPS)*. 1564–1574.
- [25] Jin-Hwa Kim, Kyoung Woon On, Woosang Lim, Jeonghee Kim, Jung-Woo Ha, and Byoung-Tak Zhang. 2017. Hadamard Product for Low-rank Bilinear Pooling. In *International Conference on Learning Representation (ICLR)*.
- [26] Diederik P Kingma and Jimmy Ba. 2014. Adam: A method for stochastic optimization. *arXiv preprint arXiv:1412.6980* (2014).
- [27] Kuang-Huei Lee, Xi Chen, Gang Hua, Houdong Hu, and Xiaodong He. 2018. Stacked cross attention for image-text matching. In *European Conference on Computer Vision (ECCV)*. 201–216.
- [28] Liunian Harold Li, Mark Yatskar, Da Yin, Cho-Jui Hsieh, and Kai-Wei Chang. 2019. Visualbert: A simple and performant baseline for vision and language. *arXiv preprint arXiv:1908.03557* (2019).
- [29] Hanxiao Liu, Karen Simonyan, and Yiming Yang. 2018. Darts: Differentiable architecture search. *arXiv preprint arXiv:1806.09055* (2018).
- [30] Jiasen Lu, Dhruv Batra, Devi Parikh, and Stefan Lee. 2019. Vilbert: Pretraining task-agnostic visiolinguistic representations for vision-and-language tasks. In *Advances in Neural Information Processing Systems (NIPS)*. 13–23.
- [31] Junhua Mao, Jonathan Huang, Alexander Toshev, Oana Camburu, Alan L Yuille, and Kevin Murphy. 2016. Generation and comprehension of unambiguous object descriptions. In *IEEE International Conference on Computer Vision (ICCV)*. 11–20.
- [32] Hyeonseob Nam, Jung-Woo Ha, and Jeonghee Kim. 2017. Dual attention networks for multimodal reasoning and matching. In *IEEE Conference on Computer Vision and Pattern Recognition (CVPR)*. 299–307.
- [33] Duy-Kien Nguyen and Takayuki Okatani. 2018. Improved Fusion of Visual and Language Representations by Dense Symmetric Co-Attention for Visual Question Answering. *IEEE Conference on Computer Vision and Pattern Recognition (CVPR)* (2018), 6087–6096.
- [34] Jeffrey Pennington, Richard Socher, and Christopher D Manning. 2014. Glove: Global Vectors for Word Representation. In *Conference on Empirical Methods in Natural Language Processing (EMNLP)*, Vol. 14. 1532–1543.
- [35] Juan-Manuel Pérez-Rúa, Valentin Vielzeuf, Stéphane Pateux, Moez Baccouche, and Frédéric Jurie. 2019. Mfas: Multimodal fusion architecture search. In *IEEE Conference on Computer Vision and Pattern Recognition (CVPR)*. 6966–6975.
- [36] Hieu Pham, Melody Guan, Barret Zoph, Quoc Le, and Jeff Dean. 2018. Efficient Neural Architecture Search via Parameters Sharing. In *International Conference on Machine Learning (ICML)*. 4095–4104.
- [37] Bryan A Plummer, Liwei Wang, Chris M Cervantes, Juan C Caicedo, Julia Hockenmaier, and Svetlana Lazebnik. 2015. Flickr30k entities: Collecting region-to-phrase correspondences for richer image-to-sentence models. In *Proceedings of the IEEE international conference on computer vision*. 2641–2649.
- [38] Shaoqing Ren, Kaiming He, Ross Girshick, and Jian Sun. 2015. Faster r-cnn: Towards real-time object detection with region proposal networks. In *Advances in neural information processing systems (NIPS)*. 91–99.
- [39] Anna Rohrbach, Marcus Rohrbach, Ronghang Hu, Trevor Darrell, and Bernt Schiele. 2016. Grounding of textual phrases in images by reconstruction. In *European Conference on Computer Vision (ECCV)*. 817–834.
- [40] David R So, Chen Liang, and Quoc V Le. 2019. The evolved transformer. *arXiv preprint arXiv:1901.11117* (2019).
- [41] Hao Tan and Mohit Bansal. 2019. LXMERT: Learning Cross-Modality Encoder Representations from Transformers. In *Conference on Empirical Methods in Natural Language Processing (EMNLP)*. 5103–5114.
- [42] Damien Teney, Peter Anderson, Xiaodong He, and Anton Van Den Hengel. 2018. Tips and tricks for visual question answering: Learnings from the 2017 challenge. In *IEEE Conference on Computer Vision and Pattern Recognition (CVPR)*. 4223–4232.
- [43] Ashish Vaswani, Noam Shazeer, Niki Parmar, Jakob Uszkoreit, Llion Jones, Aidan N Gomez, Lukasz Kaiser, and Illia Polosukhin. 2017. Attention is all you need. In *Advances in Neural Information Processing Systems (NIPS)*. 6000–6010.

- [44] Zihao Wang, Xihui Liu, Hongsheng Li, Lu Sheng, Junjie Yan, Xiaogang Wang, and Jing Shao. 2019. CAMP: Cross-Modal Adaptive Message Passing for Text-Image Retrieval. In *IEEE International Conference on Computer Vision (ICCV)*. 5764–5773.
- [45] Kelvin Xu, Jimmy Ba, Ryan Kiros, Kyunghyun Cho, Aaron C Courville, Ruslan Salakhutdinov, Richard S Zemel, and Yoshua Bengio. 2015. Show, Attend and Tell: Neural Image Caption Generation with Visual Attention. In *International Conference on Machine Learning (ICML)*, Vol. 14. 77–81.
- [46] Sibe Yang, Guanbin Li, and Yizhou Yu. 2019. Dynamic graph attention for referring expression comprehension. In *IEEE International Conference on Computer Vision (ICCV)*. 4644–4653.
- [47] Licheng Yu, Zhe Lin, Xiaohui Shen, Jimei Yang, Xin Lu, Mohit Bansal, and Tamara L Berg. 2018. Mattnet: Modular attention network for referring expression comprehension. In *IEEE Conference on Computer Vision and Pattern Recognition (CVPR)*. 1307–1315.
- [48] Licheng Yu, Patrick Poirson, Shan Yang, Alexander C Berg, and Tamara L Berg. 2016. Modeling context in referring expressions. In *European Conference on Computer Vision (ECCV)*. Springer, 69–85.
- [49] Licheng Yu, Hao Tan, Mohit Bansal, and Tamara L Berg. 2017. A joint speaker-listener-reinforcer model for referring expressions. In *IEEE Conference on Computer Vision and Pattern Recognition (CVPR)*. 7282–7290.
- [50] Zhou Yu, Yuhao Cui, Jun Yu, Dacheng Tao, and Qi Tian. 2019. Multimodal Unified Attention Networks for Vision-and-Language Interactions. *arXiv preprint arXiv:1908.04107* (2019).
- [51] Zhou Yu, Jun Yu, Yuhao Cui, Dacheng Tao, and Qi Tian. 2019. Deep Modular Co-Attention Networks for Visual Question Answering. In *IEEE Conference on Computer Vision and Pattern Recognition (CVPR)*. 6281–6290.
- [52] Zhou Yu, Jun Yu, Jianping Fan, and Dacheng Tao. 2017. Multi-modal Factorized Bilinear Pooling with Co-Attention Learning for Visual Question Answering. *IEEE International Conference on Computer Vision (ICCV)* (2017), 1839–1848.
- [53] Zhou Yu, Jun Yu, Chenchao Xiang, Jianping Fan, and Dacheng Tao. 2018. Beyond Bilinear: Generalized Multimodal Factorized High-Order Pooling for Visual Question Answering. *IEEE Transactions on Neural Networks and Learning Systems* 29, 12 (2018), 5947–5959.
- [54] Zhou Yu, Jun Yu, Chenchao Xiang, Zhou Zhao, Qi Tian, and Dacheng Tao. 2018. Rethinking Diversified and Discriminative Proposal Generation for Visual Grounding. *International Joint Conference on Artificial Intelligence (IJCAI)* (2018).
- [55] Ben P Yuhua, Moise H Goldstein, and Terrence J Sejnowski. 1989. Integration of acoustic and visual speech signals using neural networks. *IEEE Communications Magazine* 27, 11 (1989), 65–71.
- [56] Hanwang Zhang, Yulei Niu, and Shih-Fu Chang. 2018. Grounding Referring Expressions in Images by Variational Context. In *The IEEE Conference on Computer Vision and Pattern Recognition (CVPR)*.
- [57] Zhedong Zheng, Liang Zheng, Michael Garrett, Yi Yang, and Yi-Dong Shen. 2017. Dual-path convolutional image-text embedding with instance loss. *arXiv preprint arXiv:1711.05535* (2017).
- [58] Barret Zoph and Quoc V Le. 2016. Neural architecture search with reinforcement learning. *arXiv preprint arXiv:1611.01578* (2016).
- [59] Barret Zoph, Vijay Vasudevan, Jonathon Shlens, and Quoc V Le. 2018. Learning transferable architectures for scalable image recognition. In *IEEE conference on Computer Vision and Pattern Recognition (CVPR)*. 8697–8710.